

Sergey A. Khaibrakhmanov* and Alexander E. Dudorov

Dynamics of magnetic flux tubes in accretion disks of Herbig Ae/Be stars

DOI: DOI

Received ..; revised ..; accepted ..

Abstract: The dynamics of magnetic flux tubes (MFTs) in the accretion disk of typical Herbig Ae/Be star with fossil large-scale magnetic field is modeled taking into account the buoyant and drag forces, radiative heat exchange with the surrounding gas, and the magnetic field of the disk. The structure of the disk is simulated using our magnetohydrodynamic (MHD) model, taking into account the heating of the surface layers of the disk with the stellar radiation. The simulations show that MFTs periodically rise from the innermost region of the disk with speeds up to $10 - 12 \text{ km s}^{-1}$. MFTs experience decaying magnetic oscillations under the action of the external magnetic field near the disk's surface. The oscillation period increases with distance from the star and initial plasma beta of the MFT, ranging from several hours at $r = 0.012 \text{ au}$ up to several months at $r = 1 \text{ au}$. The oscillations are characterized by pulsations of the MFT's characteristics including its temperature. We argue that the oscillations can produce observed IR-variability of Herbig Ae/Be stars, which would be more intense than in the case of T Tauri stars, since the disks of Herbig Ae/Be stars are hotter, denser and have stronger magnetic field.

Keywords: accretion discs, MHD, ISM: magnetic fields, stars: variables: T Tauri, Herbig Ae/Be

1 Introduction

Accretion disks are commonly observed around young stars. Analysis of contemporary observational data shows that accretion disks of young stars (ADYSs) evolve into protoplanetary disks (PPDs), in which conditions are favourable for planet formation.

Polarization mapping of accretion disks and PPDs shows that they have large-scale magnetic field with complex geometry (Li et al., 2016). Outflows and jets, which are ubiquitous in ADYSs, are indirect signs of the large-scale magnetic field in the system (see review by Frank et al., 2014). Robust measurements of the magnetic field strength in ADYSs are still not possible. There are indications that the magnetic field can be dynamically strong near the inner edge of the disk (Donati et al., 2005). Analysis of the observational constraints on magnetic field strength from measurements of the remnant magnetization of meteorites (Levi, 1978) and Zeeman splitting of the CN lines (Vlemmings et al., 2019) shows that the magnetic field strength decreases with distance from the star. The observational data confirm predictions of the theory of fossil magnetic field, according to which the large-scale magnetic field of the accretion disks of young stars is the fossil field of the parent protostellar

clouds (Dudorov, 1995; Dudorov and Khaibrakhmanov, 2015).

MHD modeling of ADYSs have shown that strong toroidal magnetic field is generated in the innermost region of the ADYS, where thermal ionization operates and magnetic field is frozen in gas (Dudorov and Khaibrakhmanov, 2014). Runaway generation of the magnetic field in this region can be balanced by magnetic field buoyancy leading to the formation of magnetic flux tubes (MFTs), that float from the disk and carry away excess of its magnetic flux (Khaibrakhmanov and Dudorov, 2017). MFTs form in a process of magnetic buoyancy instability (also known as Parker instability, Parker, 1979) in the stratified disk with strong planar magnetic field. Formation of MFT has been found both in MHD simulations of solar interior (Vasil and Brummell, 2008) and simulations of the accretion disks (Takasao et al., 2018).

Parker instability and rising MFTs can have different manifestations in the accretion disks (see review in Dudorov et al., 2019). Khaibrakhmanov et al. (2018) and Dudorov et al. (2019) have shown that rising MFTs oscillate under certain conditions, and the oscillations can be the source of infrared (IR) variability of accretion disks of T Tauri stars (TTs). In this work, we further develop approach of Dudorov and Khaibrakhmanov and model

the dynamics of the MFT in the accretion disk of typical Herbig Ae/Be star (HAeBeS).

Structure of the paper is following. In section 2, we outline the problem statement, describe our model of the dynamics of the MFT as well as the accretion disk model. In section 3.1, we present results of the simulations of the accretion disk structure. The structure of the disk of the HAeBeS is compared with those of the TTS. Section 3.2 is devoted to the investigation of the dynamics of the MFT in absence of external magnetic field. Effect of the external magnetic field leading to magnetic oscillations of the MFT is investigated in section 3.3. We summarize and discuss our results in section 4.

2 Model

2.1 Problem statement

We consider a toroidal MFT formed inside the accretion disk in the region of effective generation of the magnetic field. The dynamics of unit length MFT is modeled in the slender flux tube approximation. Cylindrical coordinates are adopted, $(r, 0, z)$, where r is the radial distance from the center of the star, z is the height above the midplane of the disk. The MFT is characterized by radius-vector $\mathbf{r} = (r, 0, z)$, velocity vector $\mathbf{v} = (0, 0, v)$, cross-section radius a , density ρ , temperature T , and internal magnetic field strength B . The disk has density ρ_e , temperature T_e , pressure P_e and magnetic field strength B_e . The MFT starts its motion at some radial distance r from the star and a height z_0 above the disk's midplane, $z = 0$. The MFT moves in the z -direction under the action of buoyant and drag forces.

2.2 Main equations

We follow Dudorov et al. (2019) and use the system of equations describing the MFT dynamics taking into account the buoyant force, turbulent and aerodynamic drag, radiative heat exchange with the external gas, magnetic

pressure of the disk,

$$\frac{d\mathbf{v}}{dt} = \left(1 - \frac{\rho_e}{\rho}\right) \mathbf{g} + \mathbf{f}_d, \quad (1)$$

$$\frac{d\mathbf{r}}{dt} = \mathbf{v}, \quad (2)$$

$$M_1 = \rho\pi a^2, \quad (3)$$

$$\Phi = \pi a^2 B, \quad (4)$$

$$dQ = dU + P_e dV, \quad (5)$$

$$P + \frac{B^2}{8\pi} = P_e, \quad (6)$$

$$\frac{dP_e}{dz} = -\rho_e g_z, \quad (7)$$

$$U = \frac{P_e}{\rho(\gamma - 1)} + \frac{B^2}{8\pi\rho}, \quad (8)$$

where \mathbf{f}_d is the drag force, $M_1 = \text{const}$ is the mass per unit length of the MFT, $\Phi = \text{const}$ is the magnetic flux of the MFT, Q is the quantity of heat per unit mass of the MFT, U is the energy of the MFT per unit mass, g_z is the vertical component of stellar gravity, γ is the adiabatic index.

Equations of motion (1, 2) determine dependences $\mathbf{v}(t)$ and $\mathbf{r}(t)$. Differential equations describing evolution of the MFT's density and temperature can be deduced by taking time derivative of the energy equation (5) and pressure balance (6) and using the equation of the hydrostatic equilibrium of the disk (7). We define the rate of heat exchange as $h_c = dQ/dt$ and estimate it in the diffusion approximation,

$$h_c \simeq -\frac{4}{3\kappa_R\rho^2} \frac{\sigma_R T^4 - \sigma_R T_e^4}{a^2}. \quad (9)$$

where κ_R is the Rosseland mean opacity adopted from Semenov et al. (2003), σ_R is the Stefan-Boltzmann constant.

We introduce non-dimensional variables

$$\begin{aligned} u &= v/v_a, & \tilde{z} &= z/H, & \tilde{T} &= T/T_m, \\ \tilde{\rho} &= \rho/\rho_m, & \tilde{t} &= t/t_A, & \tilde{h}_c &= h_c/h_m, \\ \tilde{a} &= a/H, & \tilde{B} &= B/B_e, & \tilde{g} &= g_z/f_a, \\ \tilde{f}_d &= f_d/f_a, & \tilde{P} &= P/(\rho_m v_a^2), \end{aligned} \quad (10)$$

where v_a is the Alfvén speed, $t_A = H/v_a$ is the Alfvén crossing time, $h_m = \varepsilon_m/t_A$, ε_m is the energy density of magnetic field, $f_a = v_a/t_A$. All scales are defined at the midplane of the disk. Then the final equations of the MFT

dynamics can be written as (tilde signs are omitted)

$$\frac{du}{dt} = \left(1 - \frac{\rho_e}{\rho}\right)g + f_d, \quad (11)$$

$$\frac{dz}{dt} = u, \quad (12)$$

$$\frac{dT}{dt} = \frac{2(\gamma-1)}{\beta} \times \frac{h_c \left(\frac{\beta}{2}T + C_m \rho \right) + \rho_e g u \left(\frac{C_m}{2} - \frac{P_e}{\rho} \right)}{\frac{3-\gamma}{2}C_m \rho + \frac{\beta}{2}T + (\gamma-1)\frac{P_e}{\rho}}, \quad (13)$$

$$\frac{d\rho}{dt} = -\frac{\rho_e g u + (\gamma-1)h_c \rho}{\frac{3-\gamma}{2}C_m \rho + \frac{\beta}{2}T + (\gamma-1)\frac{P_e}{\rho}}, \quad (14)$$

$$a = C_a \rho^{-1/2}, \quad (15)$$

$$B = C_B \rho, \quad (16)$$

where β is the midplane plasma beta, $C_m = B_0^2/4\pi\rho_0^2$, $C_a = \tilde{a}_0\tilde{\rho}_0^{1/2}$, $C_B = \tilde{B}_0/\tilde{\rho}_0$.

Ordinary differential equations (11–14) together with the algebraic equations (15, 16) form closed system of equations describing the dynamics of the MFT. Equations (11–14) are supplemented by the initial conditions $u(t=0) = 0$, $z(t=0) = z_0$, $T(t=0) = T_e$, $\rho(t=0) = \rho_0$, $a(t=0) = a_0$, $B(t=0) = B_0$. Values z_0 and a_0 are the free parameters of the model, while the initial density ρ_0 is calculated from the pressure balance (6) at $t=0$. Initial magnetic field strength B_0 is specified through the initial plasma beta inside the MFT, β_0 , which is also a free parameter.

2.3 Model of the disk

The distributions of the density, temperature and magnetic field in the disk are calculated using our MHD model of the AD (Dudorov and Khaibrakhmanov, 2014; Khaibrakhmanov et al., 2017). The disk is considered to be geometrically thin and optically thick with respect to its own radiation. The mass of the disk is small compared to the stellar mass M . Inner radius of the disk is equal to the radius of stellar magnetosphere. Outer radius of the disk is determined as the contact boundary with the external medium.

The model is the generalization of Shakura and Sunyaev (1973) model. In addition to the solution of Shakura and Sunyaev (1973) equations for the low-temperature opacities, we solve the induction equation for magnetic field taking into account Ohmic dissipation, magnetic ambipolar diffusion, magnetic buoyancy and the Hall effect. The ionization fraction is calculated following Dudorov

and Sazonov (1987) taking into account thermal ionization, shock ionization by cosmic rays, X-rays and radionuclides, as well as radiative recombinations and recombinations onto dust grains.

Vertical structure of the disk is determined from the solution of the hydrostatic equilibrium equation (7) for polytropic dependence of the gas pressure on density,

$$\rho_e(z) = \rho_m \left[1 - \left(\frac{z}{H_k} \right)^2 \right]^{\frac{1}{k-1}}, \quad (17)$$

$$T_e(z) = T_m \left[1 - \left(\frac{z}{H_k} \right)^2 \right], \quad (18)$$

where

$$H_k = \sqrt{\frac{2k}{k-1}}H, \quad (19)$$

$\rho_m = \rho_e(z=0)$, $T_m = T_e(z=0)$ are the density and temperature in the midplane of the disk, $k = 1 + 1/n$, n is the polytropic index, scale height $H = v_s/\Omega_k$,

$$\Omega_k = \sqrt{\frac{GM_\star}{r^3}} \quad (20)$$

is the Keplerian angular velocity.

We consider that there is an optically thin hydrostatic corona above the optically thick disk. The corona's temperature is determined by heating due to absorption of stellar radiation,

$$T_c = 185 \left(\frac{f}{0.05} \frac{L}{L_\odot} \right)^{1/4} \left(\frac{r}{1 \text{ au}} \right)^{-1/2} \text{ K}, \quad (21)$$

where f is the fraction of the stellar radiation flux intercepted by the disk, L is the stellar luminosity (see Akimkin et al., 2012). Transition from the disk to corona is characterized by an exponential change in temperature over the local scale height H in accordance with the results of detailed modeling of the vertical structure of the accretion disks (see Vorobyov and Pavlyuchenkov, 2017).

The model of the disk has two main parameters: turbulence parameter α and mass accretion rate \dot{M} .

2.4 Model parameters and solution method

Ordinary differential equations (11–14) of the model are solved with the Runge–Kutta scheme of the 4th order with step size control.

Initially the MFT is in thermal equilibrium with external gas at $z_0 = 0.5H$. We performed a set of simulation runs for various initial radii of the MFT a_0 , plasma beta

Table 1. Model parameters: radial distance from the star, initial cross-section radius and plasma beta of the MFT.

quantity (1)	range of values (2)	fiducial value (3)
r	0.012 – 1 au	0.5 au
a_0	0.01 – 0.4 H	0.1 H
β_0	0.01 – 10	1

β_0 and radial distances from the star r . Adopted ranges of the initial parameters are listed in Table 1. Adopted fiducial value of r corresponds to the dust sublimation zone, where gas temperature is of 1500 K.

We consider the accretion disk of Herbig Ae/Be star with mass $2M_\odot$, radius $1.67R_\odot$, luminosity $11.2L_\odot$, surface magnetic field strength 1 kG, accretion rate $\dot{M} = 10^{-7}M_\odot/\text{yr}$, and turbulence parameter $\alpha = 0.01$. Adopted parameters correspond to the star MWC 480 (Donehew et al., 2011; Hubrig et al., 2011). Ionization and magnetic diffusivity parameters are adopted from the fiducial run in Khaibrakhmanov et al. (2017).

3 Results

3.1 Radial structure of the disk

First of all, let us consider the structure of the accretion disk of HAeBeS in comparison with the structure of the disk of typical TTS according to our simulations. Detailed discussion of the structure of TTS disks can found in our previous papers (Dudorov and Khaibrakhmanov, 2014; Khaibrakhmanov et al., 2017).

In Figure 1, we plot the radial profiles of midplane temperature T_m , gas surface density Σ , midplane ionization fraction x and magnetic field strength B_z .

Figure 1 shows that the structures of the accretion disks of HAeBeS and TTS are qualitatively similar.

Temperature and surface density are decreasing functions of distance, which can be represented as piece-wise power law profiles. The local slopes of the $T_m(r)$ and $\Sigma(r)$ profiles are determined by the parameters of opacity dependence on gas density and temperature (see analysis of the analytical solution of model equations by Dudorov and Khaibrakhmanov (2014)).

The ionization fraction profiles $x(r)$ is non-monotonic and have minimum at $r_{\min} \approx 0.3$ au in the case of TTS and 1 au in the case of HAeBeS. The ionization fraction is higher closer to the star, $r < r_{\min}$, due to thermal ion-

ization of alkali metals and hydrogen. Growth of the x further from the minimum, $r > r_{\min}$, is explained by decrease in gas density and corresponding increase in the intensity of ionizing radiation by external sources. Local peak in the $x(r)$ profiles at $r \approx 1$ (TTS) and 4 au (HAeBeS) is due to evaporation of icy mantles of dust grains.

Intensity of the vertical component of the magnetic field B_z generally decreases with distance. In the region of thermal ionization, $r < r_{\min}$, the magnetic field is frozen into gas and $B_z \propto \Sigma$. In the outer region, $r > r_{\min}$ magnetic ambipolar diffusion reduces magnetic field strength by 1–2 orders of magnitude as compared to the frozen-in magnetic field. For example, magnetic field strength is of 0.1 G near the ionization minimum.

Comparison of the simulation results for HAeBeS and TTS shows that the accretion disk is hotter and denser in the former case at any given r . This is because the disk of HAeBeS has higher accretion rate, which leads to more intensive turbulent heating of the gas in the disk. As a consequence, the size of the innermost region, where runaway growth of the magnetic field is possible due to high ionization level, is more extended in the case of the HAeBeS. For adopted parameters, this region ranges from the inner boundary of the disk, $r_{\text{in}} = 0.012$ au, up to $r \approx r_{\min} = 1$ au. Magnetic field strength is greater in the case of HAeBeS.

3.2 MFT dynamics without external magnetic field

In this section we study the dynamics of the MFT in the disk of HAeBeS in absence of the magnetic field outside the MFT.

In Figure 2, we plot dependences of the MFT’s speed, density, radius and temperature on the z -coordinate at $r = 0.5$ au for different initial cross-section radii, $a_0 = 0.01, 0.1, 0.2,$ and $0.4 H$.

Figure 2(a) shows that thinner MFT, $a_0 = 0.01 H$, is characterized by three stages of evolution. First the MFT accelerates inside the disk, then it rapidly decelerates near the surface, $z \approx 2.6 H$, and after that it again rises with acceleration in the corona of the disk. Finally, the MFT dissipates in the corona, in a sense that its radius grows fast and becomes comparable with the half-thickness of the disk, as Figure 2(c) shows. Hence, MFTs will form outflowing magnetized corona of the disk, as in the case of TTS discussed by Dudorov et al. (2019). The MFT of intermediate initial radii, $a_0 \sim 0.1 - 0.2 H$, rise with higher speed, $v \approx 1 - 2 \text{ km s}^{-1}$, and dissipate right after

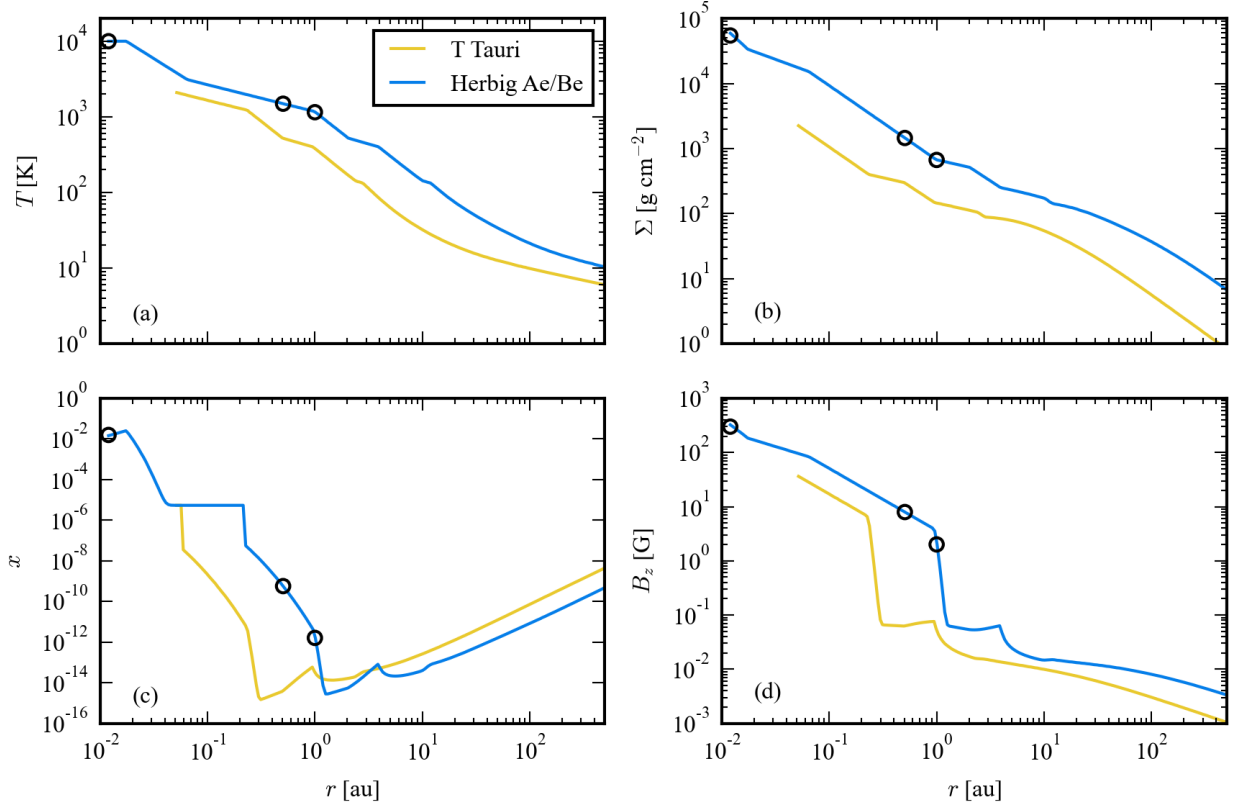


Fig. 1. Radial profiles of the midplane temperature (a), surface density (b), midplane ionization fraction (c) and midplane magnetic field strength (d) in the accretion disks of typical T Tauri star (yellow lines) and Herbig Ae/Be star (blue lines). Empty circle markers show the points at which the modeling of the dynamics of the MFT was performed.

rising to the corona without proceeding to the stage of further acceleration. Thick MFT with $a_0 = 0.4H$ float with highest speeds up to 3 km s^{-1} and dissipate near the surface of the disk.

Upward motion of the MFT is caused by the buoyancy force, which depends on the difference between internal and external densities, $\Delta\rho = \rho_e - \rho$. Figure 2(b) shows that $\Delta\rho > 0$ and therefore the buoyant force is positive in all considered cases. The MFT expands and its density decreases during its motion in order to sustain the pressure balance. Near the surface of the disk and in the corona, $\Delta\rho$ approaches zero and therefore the MFT's speed decreases. Abrupt deceleration of the MFT after passing the surface of the disk, is caused by the abrupt disk's density drop in this region of transition from the disk to corona.

The MFT stays in thermal equilibrium, $T \approx T_e$, during upward motion inside the disk, as Figure 2(d) shows. This is due to fast radiative heat exchange with the external gas. Departure from thermal equilibrium is observed

only for the MFTs with $a_0 = 0.1 - 0.2H$ after their rising from the disk to the transition region, where T_e grows up to the corona's temperature of 475 K.

In Figure 3, we plot the dependence of the MFT's speed on the z -coordinate at $r = 0.5 \text{ au}$ for $z_0 = 0.5H$, $a_0 = 0.1H$, and various initial plasma beta β_0 . Figure 3 shows that the MFT with stronger magnetic field accelerate to greater speed. Maximum speed of $7 - 8 \text{ km s}^{-1}$ is achieved by the MFT with $\beta_0 = 0.01$. The increase of the MFT's speed with β_0 is explained by the fact, that the more initial magnetic field strength of the MFT, the more initial $\Delta\rho$ and correspondingly the buoyant force is stronger. Closer to the star, $r < 0.5 \text{ au}$, the maximum speed is of $10 - 12 \text{ km s}^{-1}$, according to our simulations.

3.3 Magnetic oscillations

In this section we investigate, how does the magnetic pressure outside the MFT influences its dynamics. In this

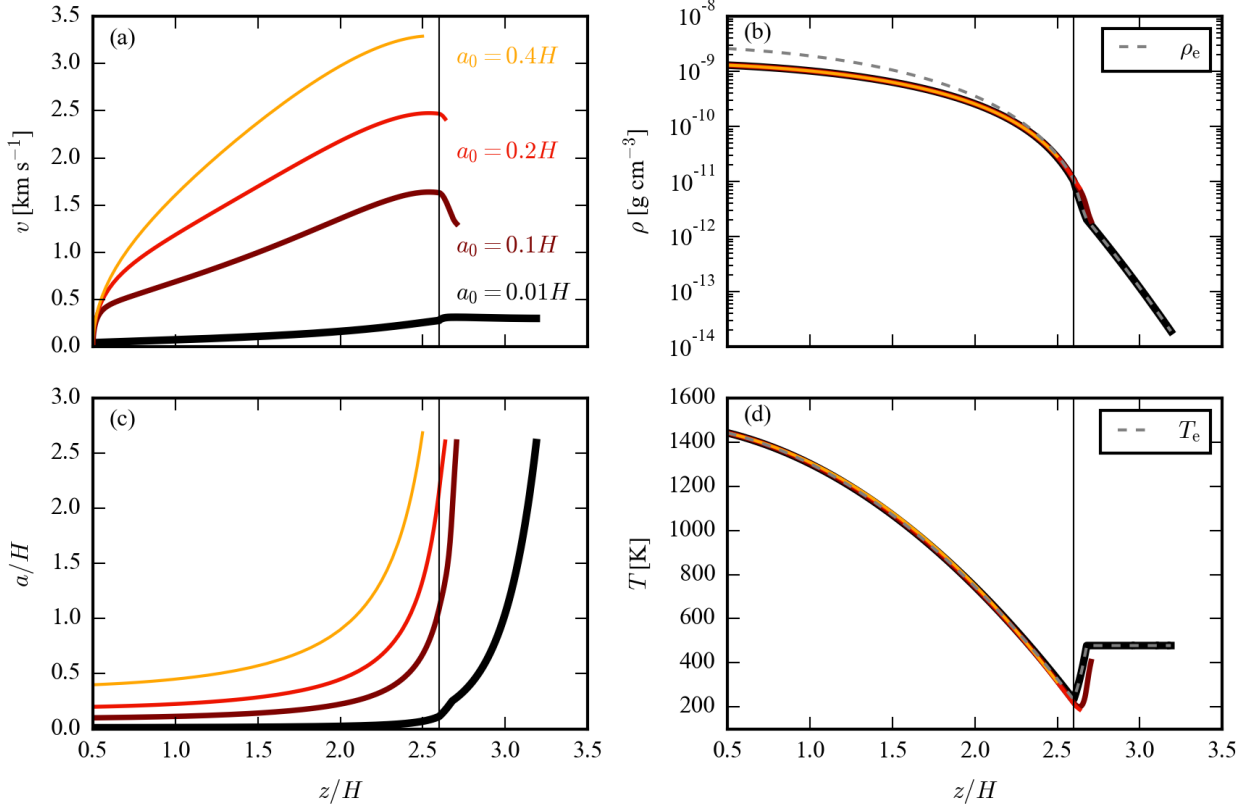


Fig. 2. Dynamics of the MFTs of various initial cross-section radii a_0 in absence of the external magnetic field. Dependences of the MFT's speed (panel a), density (b), cross-section radius (c) and temperature (d) on the z -coordinate are shown. Vertical lines show the surface of the disk. Grey dashed lines in panels (b) and (d) delineate corresponding profiles of the disk's density and temperature. Initial parameters of the MFT: $r = 0.5$ au, $z_0 = 0.5 H$, and $\beta_0 = 1$.

case, external pressure P_e in (6) is a sum of gas pressure and magnetic pressure $B_e^2/8\pi$. We assume that B_e is constant with z and has magnitude of B_z .

In Figure 4, we present simulation results for the MFT at $r = 0.5$ au with fiducial $z_0 = 0.5 H$, $a_0 = 0.1 H$ and various initial plasma beta, β_0 . The dependences of MFT's speed, density, radius and temperature on the z -coordinate are depicted. Magnetic field strength is of 8 G at considered r .

Figure 4 shows that the dynamics of the MFT differs from the case with zero external magnetic field. The MFT floats with acceleration up to some height z_o near the surface of the disk, and then its motion becomes oscillatory: the MFT moves vertically up and down around the point z_o . According to Figure 4(a), $z_o \approx 2.2, 2.5$, and $2.6 H$ for $\beta_0 = 1, 0.1$, and 0.01 , respectively. Hence, the more β_0 the higher the point z_o , around which the MFT oscillates. Magnitude of the MFT's speed decreases during oscillations as the MFT loses its kinetic energy due to the friction with the external gas.

When the MFT starts to oscillate, its expansion stops at some characteristic cross-section radius a_o . In the considered case, this radius is of $0.3 H$, according to Figure 4(c). The radius of the MFT periodically increases and decreases with respect to a_o during the oscillations, i. e. the MFT pulsates. The magnitude of the radius variations decreases, i. e. the pulsations decay with time.

Figure 4(b) shows that the point z_o is a point of zero buoyancy, such that $\Delta\rho = \rho_e - \rho > 0$ at $z < z_o$ and $\Delta\rho < 0$ at $z > z_o$. This effect is caused by the contribution of the magnetic pressure outside the MFT to the overall pressure balance (6). The external magnetic field B_e is constant with z , while the density of the disk ρ_e exponentially decreases. As a consequence, the magnetic pressure $B_e^2/8\pi$ contribution to P_e also increases in comparison to the gas pressure. At $z \geq z_o$, the external magnetic field becomes stronger than the magnetic field of the MFT, and consequently the MFT becomes heavier than the external gas. This result is similar to that found

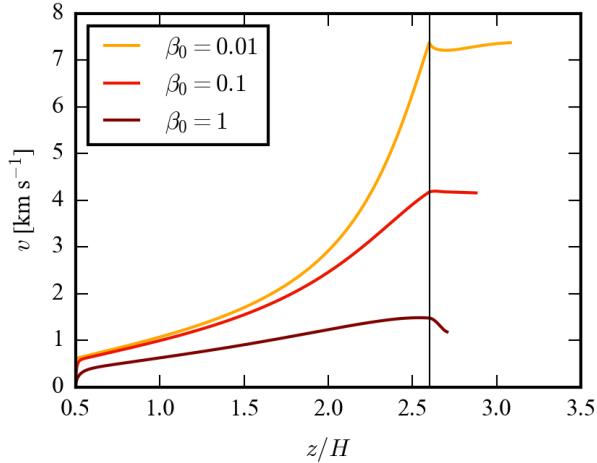


Fig. 3. Dependence of the MFT’s speed on the z -coordinate for various initial plasma beta β_0 in runs without external magnetic field. Vertical line delineates the surface of the disk. Initial parameters: $r = 0.5$ au, $z_0 = 0.5 H$, and $a_0 = 0.1 H$.

by Dudorov et al. (2019) for the MFT in the accretion disks of TTS.

The beginning of the magnetic oscillations is characterized by violation of the thermal balance, $T \neq T_e$, as Figure 4(d) shows. This means that the rate of radiative heat exchange is smaller than the rate of MFT’s cooling due to adiabatic expansion. During the oscillations, the MFT’s pulsations decay and radiative heat exchange ultimately equalizes the temperature T and T_e .

In Figure 5, we plot corresponding dependences of MFT’s temperature on time. Figure 5 clearly demonstrates the periodic changes in MFT’s temperature during the magnetic oscillations. The period of oscillations increases with β_0 and lies in range from 0.5 month for $\beta_0 = 0.01$ to 2 months for $\beta_0 = 1$.

Picture of the MFT’s thermal evolution in the case $\beta_0 = 1$ can be described as simple decaying oscillations. In this case, the oscillations take place under the surface of the disk (see Figure 4(a)), and the MFT’s temperature follows the polytropic disk’s temperature profile during its periodic upward and downward motion. The MFTs with $\beta_0 \leq 0.1$ exhibit more complex behaviour characterized by non-harmonic oscillations of the temperature. In the case $\beta_0 = 0.01$, the maximum of each temperature pulsation is characterized by a constant $T = 475$ K during time interval of 0.1 – 0.5 months. Such a behaviour is explained by the fact, that the MFT’s with $\beta_0 \leq 0.1$ oscillate near the surface of the disk. The vertical profile of disk’s temperature is non-monotonic in this region with

minimum at z_s , according to Figure 4(d). Therefore, the maximum T in the oscillating MFT corresponds to the corona’s temperature of 475 K, while the minimum T is achieved at some point below the surface of the disk.

In order to investigate characteristic time scales of this process, we plot the dependence of the z -coordinate, temperature and magnetic field strength of the MFT on time in Figure 6. The results for the MFT with fiducial parameters $z_0 = 0.5 H$, $a_0 = 0.1 H$, and $\beta_0 = 1$ at various radial distances from the star are shown. Considered radial distances are marked with empty circles in $T(r)$, $\Sigma(r)$, $x(r)$, and $B(r)$ profiles in Figure 1.

Figures 6(a, b, c) show that the magnetic oscillations take place beneath the surface of the disk, at $z \sim 2 - 2.5 H$ typically. The oscillations are found at every radial distance in the considered range, $r = 0.012 - 1$ au. The period of oscillations P_o increases with r , such that $P_o \approx 0.2$ d ≈ 5 hrs at $r = 0.012$ au, 2 months at $r = 0.5$ au, and 5 months at $r = 1$ au. The amplitude of upward and downward motion decreases with time.

According to Figures 6(d, e, f), the magnetic oscillations are accompanied by corresponding periodic changes in the MFT’s temperature. The MFT heats up during the period of downward motion and cools down during its upward motion. These changes reflect the z -distribution of the disk’s temperature T_e , since the radiative heat exchange tends to keep the MFT in thermal balance with the external gas. The magnitude of the temperature fluctuations decreases with r . In maximum, it ranges from $\Delta T \sim 3000$ K at $r = 0.012$ au to 300 K at $r = 1$ au.

Dependences $B(t)$ depicted in Figures 6(d, e, f) show that the MFT’s magnetic field strength decreases during its upward motion up to a point of the zero buoyancy. This decrease reflects the expansion of the MFT, $B \propto a^{-2}$ according to the magnetic flux conservations. During the following magnetic oscillations, the magnetic field strength periodically increases and decreases with respect to the value B_e . This picture confirm above discussions that the magnetic oscillations arise due to the effect of external magnetic pressure near the point of zero buoyancy, which is characterized by the equality $B \approx B_e$.

4 Conclusions and discussion

We numerically modeled the dynamics of MFTs in the accretion disk of typical HAeBeS. The simulations were carried out in frame of the slender flux tube approximations using the model developed by Dudorov et al. (2019). This models allows to investigate the motion of the MFT

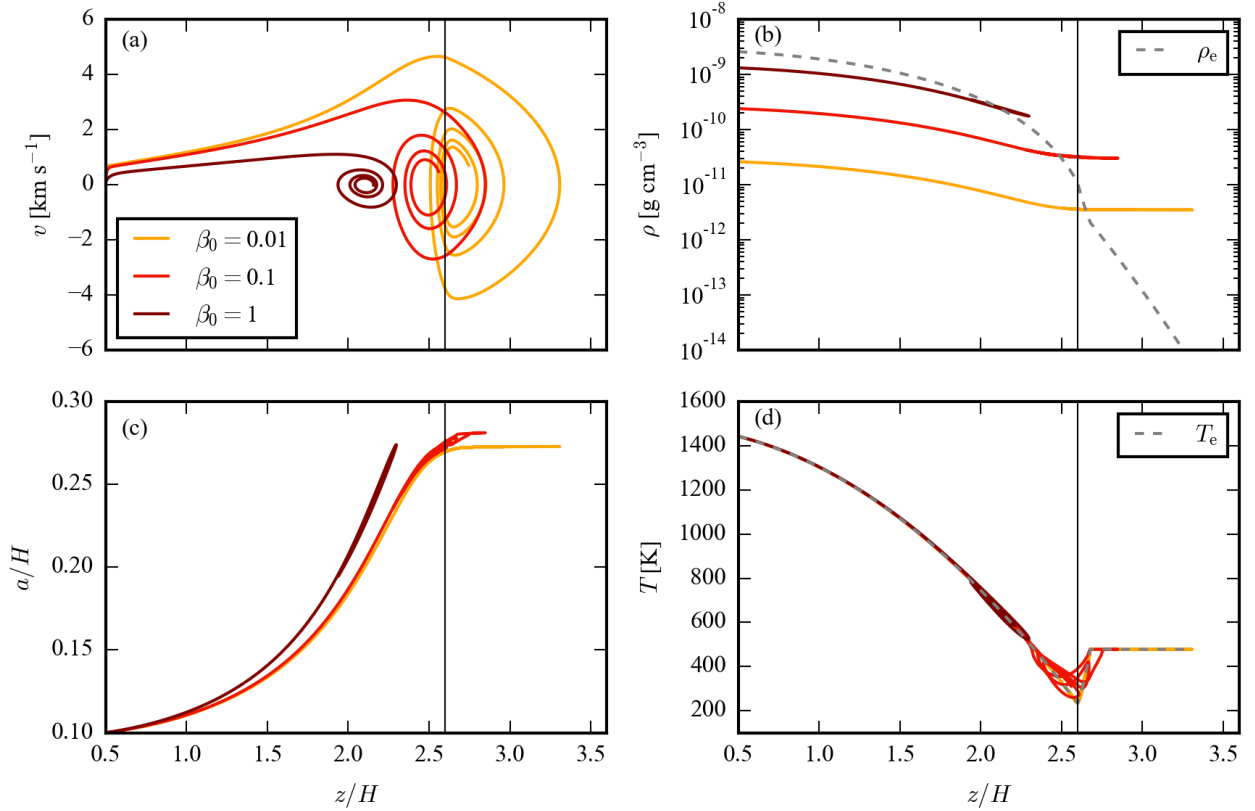


Fig. 4. Dynamics of MFTs with various initial plasma beta β_0 in presence of external magnetic field. Dependences of the MFT's speed (panel a), density (b), cross-section radius (c) and temperature (d) on the z -coordinate are plotted. Vertical lines show the surface of the disk. Grey dashed lines in panels (b) and (d) delineate corresponding profiles of the disk density and temperature. Initial parameters: $r = 0.5$ au, $z_0 = 0.5 H$, and $a_0 = 0.1 H$.

in the direction perpendicular to the disk's plane taking into account the buoyant and drag forces, radiative heat exchange of the MFT with external gas, magnetic pressure of the disk.

The structure and characteristics of the accretion disk were calculated using our MHD model of the accretion disks (see Khaibrakhmanov et al., 2017), which is based on the model of Shakura and Sunyaev (1973). The vertical structure of the disk at each radial distance r is calculated from the solution of the hydrostatic equilibrium equation for the case of polytropic gas. It is considered that the turbulent friction is the main heating mechanism inside the disk. There is optically thin corona above the optically thick disk. The temperature of the corona is determined by the heating of the gas with incident stellar radiation. We adopted that the fraction of the radiation flux intercepted by the disk's surface is constant, $f = 0.05$, at every r . Transition from the disk to its corona is treated as hydrostatic region with exponential growth of gas temperature over the local scale height of the disk.

We adopted the parameters of the star and its accretion disk corresponding to the star MWC 480. This is a typical 'isolated' HAeBeS, which was investigated in detail in different spectral ranges (see Fernandez et al., 2018; Mendigutía et al., 2013; Sitko et al, 2008; Tambovtseva et al., 2016).

Our simulations have shown that the accretion disk of the HAeBeS is in general larger, denser and hotter than the accretion disk of typical TTS. This is because the disk in the former case is characterized by larger accretion rate. As a consequence, the magnetic field in the disk of HAeBeS is stronger than in the disk of TTS. The innermost region of the disk, where temperature is high enough for thermal ionization of alkali metals and hydrogen and where the magnetic field is frozen into gas, is more extended in the case of HAeBeS. This region ranges from 0.012 au up to $r = 1$ au in radial direction, under adopted parameters.

We modeled the dynamics of the MFT of various initial cross-section radii, a_0 , and plasma beta, β_0 , at several

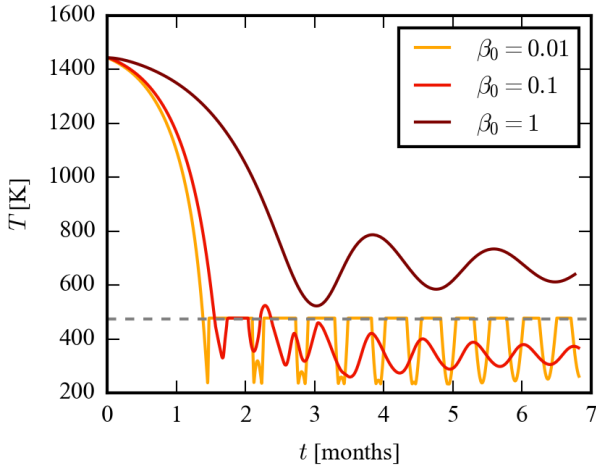


Fig. 5. Dependence of the MFT’s temperature on time for various initial plasma beta β_0 in presence of external magnetic field. Horizontal dashed line delineates the temperature of the disk’s corona. Initial parameters: $r = 0.5$ au, $z_0 = 0.5 H$, and $a_0 = 0.1 H$.

radial distances r in the range $0.012 - 1$ au. The simulations have shown that the dynamics of the MFT in the accretion disk of the HAeBeS is in general qualitatively similar to the case of typical TTS. In absence of the external magnetic field, MFTs rise from the disk with typical speeds up to $10 - 12$ km s $^{-1}$ and form outflowing magnetized corona of the disk. Radiative heat exchange rapidly equalizes the temperatures inside and outside the MFT, $T \approx T_e$, under all considered parameters. We did not found thermal oscillations of the MFT, caused by adiabaticity, unlike the case of the TTS, for which the thermal oscillations of the MFT with $a_0 \sim 0.1$ and $\beta_0 = 1$ at $r < 0.2$ au were found by Dudorov et al. (2019). Like in the case of TTS, MFTs transport excess of the disk’s magnetic flux into its corona.

The pressure of the magnetic field outside the MFT halts upward motion of the MFT near the point, where internal and external magnetic fields are nearly equal. This point of zero buoyancy, z_o , typically lies near the surface of the disk, $z_s \sim 2.5 - 3 H$, where H is the local isothermal scale height. The more initial magnetic field strength of the MFT, the higher the point z_o lies. After the MFT rises to this point, its motion becomes oscillatory. The MFT moves up and down around the point z_o and pulsates. The magnitude of these magnetic oscillations decreases with time because of the loss of the MFT’s kinetic energy due to friction with external gas. The period of the oscillations increases with radial distance and

ranges from few hours at the inner boundary of the disk, $r = 0.012$ au, up to several months at $r = 1$ au in the case of typical $a_0 = 0.1 H$ and $\beta_0 = 1$. The oscillation period increases with β_0 at a given r .

Correspondingly, the temperature of the MFT experiences decaying oscillations around the value of local external temperature at the point z_o . During the first few periods of the oscillations, temperatures inside and outside the MFT are not equal to each other, i. e. radiative heat exchange is not efficient, and the MFT is practically adiabatic. But ultimately the heat exchange equalizes temperature of the MFT and external gas. The maximum magnitude of the temperature variations ranges from several thousand Kelvin at the inner edge of the disk to several hundred Kelvin at $r = 1$ au. Temperature variations during each period of the oscillations may be non-harmonic and asymmetric, since the oscillations take place near the surface of the disk, where the dependence of the disk’s temperature on the z -coordinate is complex and non-monotonic.

Following original idea of Khaibrakhmanov et al. (2018), we propose that the oscillations of MFTs can be a source of the emission variability as well as variable circumstellar extinction observed in young stars with accretion disks. Such a variability is a widespread feature of the accretion disks of TTS and HAeBeS (see Flaherty et al., 2016; Kóspál et al., 2012), which also has been found for the MWC 480 star considered as a reference in our modeling. Generally speaking, periodically rising and oscillating MFTs could contribute to the variability of the emission in different spectral ranges emanating from the innermost region of the disk, where the magnetic field is frozen in into gas: $r = 0.012 - 1$ au in the case of considered HAeBeS. The MFTs formed beyond the dust sublimation radius, $r = 0.5$ au, could contain dust grains. In this case, temperature fluctuations of the oscillating MFT may cause the IR-variability of the disk. This assumption is supported by the observations of MWC 480 demonstrating the variations in the IR-flux over $1 - 13 \mu\text{m}$ wavelength range (Fernandez et al., 2018; Sitko et al, 2008). This radiation emanates from the dust sublimation zone and points to the changes of the disk’s structure in this region. It should be noted, that inhomogeneities in the disk centrifugal winds containing both gas and dust can cause the variability of young stars’ emission, in particular the variations in circumstellar extinction observed in young stars (Tambovtseva and Grinin, 2008). Application of both models to specific systems with well-established variability is needed in order to determine relative role of various variability mechanisms.

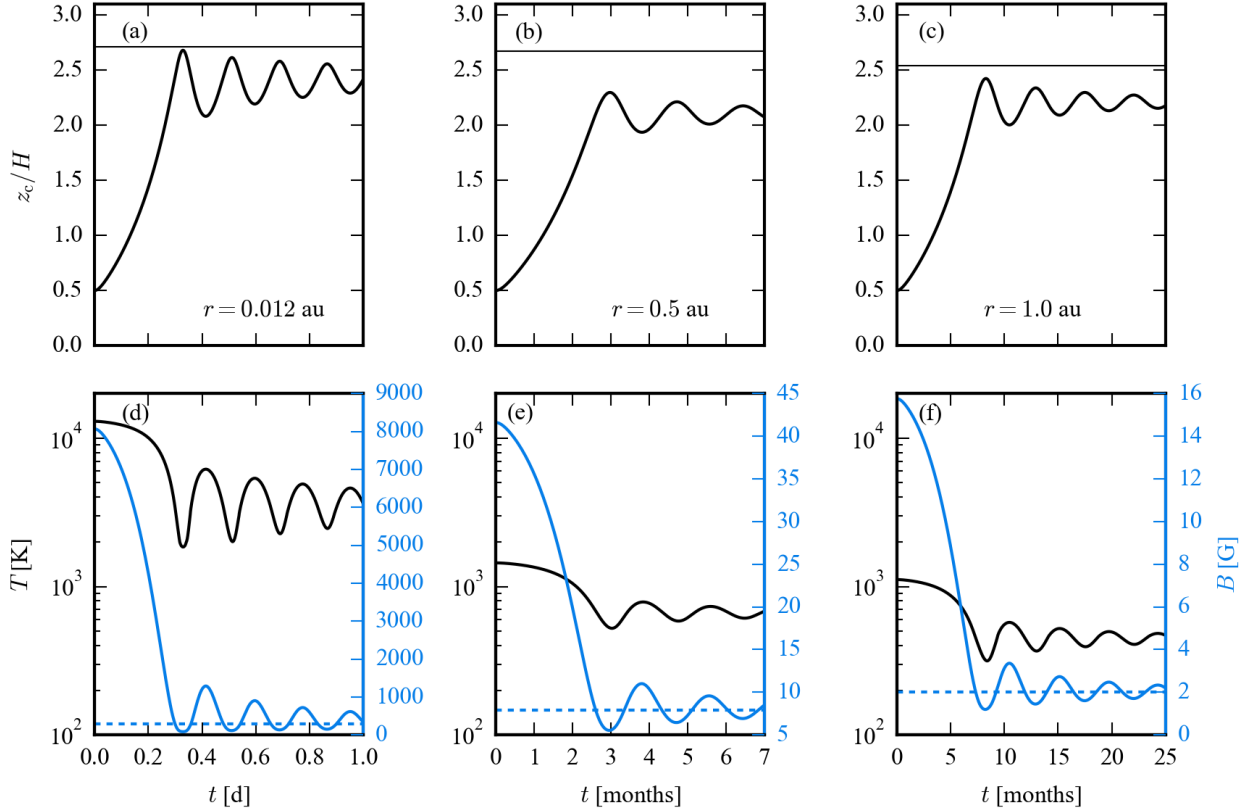


Fig. 6. Dynamics of the MFTs at different r in presence of external magnetic field. Top row: the dependence of the z -coordinate of the MFT on time during its motion inside the disk at various radial distances $r = 0.012, 0.15$ and 1 au (panels from left to right). Horizontal lines show the surface of the disk. Bottom row: corresponding dependences of temperature (left y -axis, black lines) and magnetic field strength (right y -axis, blue lines) on time. Horizontal dashed blue lines correspond to the external magnetic field B_e . Initial radius and plasma beta of the MFT are $a_0 = 0.1 H$ and $\beta_0 = 1$, respectively.

In general, our results have shown that the accretion disks of HAeBeS have more extended region of the efficient generation of the magnetic field than in the case of TTS. The temperature of their corona is higher due to more intense stellar radiation. As a consequence, temperature variations in the oscillating MFTs has larger magnitude. Therefore, the IR-variability caused by oscillating MFTs would be more intense in the case of accretion disks of HAeBeS as compared to TTS.

In order to investigate the connection between magnetic oscillations of MFTs and IR-variability of TTS and HAeBeS, we plan to calculate spectral energy distributions (SEDs) of the accretion disks taking into account variations of their structure due to the effect of rising MFTs. Interesting task is to model the synthetic light-curves of the accretion disks taking into account contribution of periodically rising MFTs into the IR flux of the disk.

Acknowledgements

Authors thank anonymous referee for useful comments. The work is supported by the Russian Science Foundation (project 19-72-10012).

References

- Akimkin VV, Pavlyuchenkov YN, Launhardt R, Bourke T. 2012. Structure of CB 26 protoplanetary disk derived from millimeter dust continuum maps. *Astron Rep.* 56(12):915–930.
- Donati J-F, Paletou F, Ferreira J. 2005. Direct detection of a magnetic field in the innermost regions of an accretion disk. *Nature.* 438:466–469.
- Donehew B, Brittain S. 2011. Measuring the Stellar Accretion Rates of Herbig Ae/Be Stars. *Astron J.* 141(2):46.
- Dudorov AE, Sazonov YV. 1987. Hydrodynamical collapse of interstellar clouds. IV. The ionization fraction and ambipolar diffusion. *Nauchnye Inform.* 63:68–86.

- Dudorov AE. 1991. Fossil magnetic fields in T Tauri stars. *Astron Rep.* 39(6):790–798.
- Dudorov AE, Khaibrakhmanov SA. 2014. Fossil magnetic field of accretion disks of young stars. *Astrophys Space Sci.* 352:103–121.
- Dudorov AE, Khaibrakhmanov SA. 2015. Theory of fossil magnetic field. *Adv Space Res.* 55:843–850.
- Dudorov AE, Khaibrakhmanov SA, Sobolev AM. 2019. Dynamics of magnetic flux tubes in accretion discs of T Tauri stars. *Mon Not R Astron Soc.* 487(4):5388–5404.
- Fernandez RB, Long ZC, Pikhartova M, Sitko ML, Grady CA, Russel RW, et al. 2018. Variability of Disk Emission in Pre-main-sequence and Related Stars. IV. Investigating the Structural Changes in the Inner Disk Region of MWC 480. *Astrophys J.* 856:103.
- Flaherty KM, DeMarchi L, Muzerolle J, Balog Z, Herbst W, Thomas S, et al. 2016. Spitzer Observations of Long-term Infrared Variability among Young Stellar Objects in Chamaeleon I. *Astrophys J.* 833(1):104.
- Frank A, Ray TP, Cabrit S, Hartigan P, Arce HG, Bacciotti F, et al. 2014. Jets and Outflows from Star to Cloud: Observations Confront Theory. In: Beuther H, Klessen RS, Dullemond CP, Henning Th, Editors. *Protostars and Planets VI*. Tucson: University of Arizona Press. p.451–474.
- Hubrig S, Schöller M, Ilyin I, Cowley CR, Mikulášek Z, Stelzer B, et al. 2011. Characterising the magnetic fields of the Herbig Ae/Be stars HD 97048, HD 150193, HD 176386, and MWC 480. *Astron Astrophys.* 536:A45.
- Khaibrakhmanov SA, Dudorov AE, Parfenov SYu, Sobolev AM. 2017. Large-scale magnetic field in the accretion discs of young stars: the influence of magnetic diffusion, buoyancy and Hall effect. *Mon Not R Astron Soc.* 464:586–598.
- Khaibrakhmanov SA, Dudorov AE. 2017. Magnetic field buoyancy in accretion disks of young stars. *Phys Part Nuclei Lett.* 14:882–875.
- Khaibrakhmanov SA, Dudorov AE, Sobolev AM. 2018. Dynamics of magnetic flux tubes and IR-variability of young stellar objects. *Res Astron Astrophys.* 18:090.
- Kóspál A, Ábrahám P., Acosta-Pulido JA, Dullemond CP, Henning Th, Kun M, et al. 2021. Mid-Infrared Spectral Variability Atlas of Young Stellar Objects. *Astrophys J Suppl S.* 201:11.
- Levi EH. 1978. Magnetic field in the primitive solar nebula. *Nature.* 276:481.
- Li D, Pantin E, Telesco CM, Zhang H, Wright CM, Barnes PJ, et al. 2016. An Ordered Magnetic Field in the Protoplanetary Disk of AB Aur Revealed by Mid-Infrared Polarimetry. *Astrophys J.* 832:18.
- Mendigutía I, Brittain S, Eiroa C, Meeus G, Montesinos B, Mora A, et al. 2013. Accretion variability of Herbig Ae/Be stars observed by X-Shooter. HD 31648 and HD 163296. *Astrophys J.* 776:44.
- Parker E. 1979. *Cosmical magnetic fields: Their origin and their activity*. Oxford: Clarendon Press. 858 p.
- Semenov D, Henning T, Helling C, Ilgner M, Sedlmayr E. 2003. Rosseland and Planck mean opacities for protoplanetary discs. *Astron Astrophys.* 410:611–621.
- Shakura NI, Sunyaev RA. 1973. Black holes in binary systems. Observational appearance. *Astron Astrophys.* 24:337–355.
- Sitko ML, Carpenter WJ, Kines RL, Wilde JL, Lynch DK, Russel RW, et al. 2008. Variability of Disk Emission in Pre-Main Sequence and Related Stars. I. HD 31648 and HD 163296 — Isolated Herbig Ae Stars Driving Herbig-Haro Flows. *Astrophys J.* 678:1070–1087.
- Takasao S, Tomida K, Iwasaki K, Suzuki TK. 2018. A Three-dimensional Simulation of a Magnetized Accretion Disk: Fast Funnel Accretion onto a Weakly Magnetized Star. *Astrophys J.* 857:4.
- Tambovtseva LV, Grinin VP. 2008. Dust in the disk winds from young stars as a source of the circumstellar extinction. *Astron Lett.* 34:231.
- Tambovtseva LV, Grinin VP, Potravnov IS, Mkrtychian DE. 2016. Disk wind and magnetospheric accretion in emission from the Herbig Ae star MWC 480. *Astron Lett.* 42:583–597.
- Turner NJ, Carballido A, Sano T. 2010. Dust transport in protostellar disks through turbulence and settling. *Astrophys J.* 708:188.
- Vasil GM, Brummell NH. 2008. Magnetic Buoyancy Instabilities of a Shear-generated Magnetic Layer. *Astrophys J.* 686:709–730.
- Vlemmings W, Lankhaar B, Cazzoletti P, Ceccobello C, Dall’Ólio D, van Dishoek EF, et al. 2019. Stringent limits on the magnetic field strength in the disc of TW Hya. *Astron Astrophys.* L7:10.
- Vorobyov EI, Pavlyuchenkov YN. 2017. Improving the thin-disk models of circumstellar disk evolution. The 2+1-dimensional model. *Astron Astrophys.* 606:A5.